Journal of Sound and Vibration 511 (2021) 116325

Contents lists available at ScienceDirect

Journal of Sound and Vibration

journal homepage: www.elsevier.com/locate/jsvi

Generalised round-trip identity—For the determination of structural dynamic properties at locations inaccessible or too distant for direct measurement

K. Wienen [a,*], M. Sturm [a], A.T. Moorhouse [b], J.W.R. Meggitt [b]

[a] Robert Bosch Automotive Steering LLC, Plymouth, MI, USA
[b] Acoustics Research Centre, University of Salford, Greater Manchester, UK

ARTICLE INFO

Keywords:
Frequency response function
Experimental structural dynamics
Transfer path analysis
Virtual acoustic prototyping
In-situ blocked force
System identification

ABSTRACT

In noise and vibration engineering, a structure's passive dynamic properties are often quantified by frequency response functions (FRFs). This paper focuses on acquiring FRFs from experimental tests, considering both, translational (x, y, z) and rotational (e.g. moments around these axes) terms. In practical applications, test structures may not allow FRFs to be measured directly due to the impracticality of applying a controlled excitation in a particular direction (e.g. in-plane), the inability to measure rotational dynamics (e.g. moment excitation), insufficient signal-to-noise ratio (SNR) between excitation and response degrees of freedom, or simply due to restricted access. Methods exist to resolve some of the mentioned issues using indirect experimental techniques, such as the round-trip identity. However, these methods are limited to cases in which the driving-point FRFs are sought-after. The present paper extends previous work into a more generalised formulation of the round-trip identity feasible for reconstructing driving-point and transfer mobilities from in-situ measurements conducted in coupled assemblies. By using the round-trip identity, the excitation of moments and/or inaccessible points is avoided altogether and instead replaced by a number of applied forces remote to the points of interest. Manipulation of this round-trip identity yields a formulation for long distance transfer FRFs, expressed in terms of multiple shorter transfer path elements, which are less prone to insufficient SNR. These practical applications of the generalised round-trip concept are experimentally validated for multi-input multi-output assemblies.

1. Introduction

To approach structure-borne sound and vibration problems in their full complexity (e.g. as multi-path and multi-degrees of freedom (DoF) systems), experimental techniques to accurately characterise the structural dynamic properties of coupled structures are of great importance. Developing accurate numerical models of the structural and/or vibro-acoustic behaviour of complex machinery is particularly challenging. Instead, experimental methods are often preferred in which the structure's dynamic properties are expressed by frequency response functions (FRFs), such as compliance, mobility or accelerance. Typically, driving-point and transfer FRFs of a structure are determined by employing roving instrumented hammers or shakers. With either kind of FRF measurement, its excitation can prove problematic, particularly in practical scenarios where access is limited. However, the correct position of an excitation is essential to obtain accurate FRF measurements. This is particularly so when considering diagnostic

* Corresponding author.
E-mail address: kevin.wienen@bosch.com (K. Wienen).

https://doi.org/10.1016/j.jsv.2021.116325
Received 15 October 2020; Received in revised form 9 April 2021; Accepted 26 June 2021
Available online 2 July 2021

methods such as transfer path analysis (TPA) [1] or the related discipline of noise and vibration predictions in virtual assemblies (e.g. Virtual Acoustic Prototyping (VAP) [2,3] or component-based TPA [4,5]). In these applications, a set of FRFs is characterised at and between the source–receiver (active–passive) interface of an assembly and some specified response positions on the passive receiver-side. The measured FRFs (both structural and vibro-acoustic) are used for the inverse identification of the blocked force (ISO 20270:2019) [6,7] and the forward response prediction to some target DoF (e.g. driver's ear). In these applications, it is well known that small errors, for example, due to inaccurate excitation positions, can lead to large uncertainties in the identified forces and corresponding response predictions [8]. This sensitivity highlights the challenges commonly encountered when characterising structural dynamic systems.

In a laboratory environment, test rigs may be specifically designed to facilitate unrestricted interface access, so that problems due to insufficient excitation positioning can be avoided. This, however, is generally not the case for most functional components when mounted in-situ. Assuming each contact behaves rigidly, the direct measurement of a complete FRF matrix requires excitations in 6 coordinate DoF, i.e. x, y and z translations alongside their corresponding rotations. Experimentally, this type of measurement is restricted by the impracticality of applying a controlled excitation in a particular direction (e.g. in-plane or moment). These practical challenges have led to a near-routine neglect of in-plane and rotational transmission paths, potentially resulting in unrealistic prognoses [9].

For inaccessible coupling interfaces (e.g. in an engine bay or other types of encapsulated sources), the principle of reciprocity may be invoked to interchange the position of response and excitation, so as to simplify a transfer function measurement [10]. Often, reciprocal FRF measurements are not possible because both the response position and at least a subset of the coupling interface DoF are inaccessible for excitation (e.g. vibro-acoustic transfer paths between engine bushings and target sound pressure probes in the vehicle cabin). Hence, there is a need for indirect methods with the ability to relocate excitations to more convenient locations remote from inaccessible interfaces.

The 'round-trip' identity proposed by Moorhouse et al. [11] establishes such an indirect relationship between the driving-point FRFs at a coupling interface, and the transfer functions surrounding it (see also [12]). This identity allows reconstructing driving-point FRFs at an interface from relocated (easy-to-access) remote measurements on the source and receiver sub-structures. Whilst the original round-trip formulation considers a conventional single interface source–receiver assembly, a subsequent derivation by Meggitt et al. [13,14] introduces a dual interface counterpart, accounting for isolator coupling. Together, the round-trip identity and its dual interface extension provide an in-situ characterisation of resilient coupling elements using only remote excitations, that is, avoiding excitation at either interface. The round-trip and its dual interface extension have found application in experimental structural dynamics, for example, due to their ability to determine in-plane driving-point FRFs. However, this indirect characterisation has been restricted to DoF on the coupling interface. In this paper, the round-trip concept is generalised to include transfer FRFs between a coupling interface and arbitrary remote points. Within this generalised concept, direct excitation of rotational DoF or inaccessible points on either side of the transfer path is avoided altogether and instead replaced by a number of rectilinear forces, which by choice of the experimentalist can be applied at accessible positions. As for the earlier methods, the DoF introduced by the generalised round-trip identity may be defined at the source–receiver interface itself to recall the standard or dual interface round-trip formulation for driving-points. By rearranging the proposed generalised formulation, an interesting relationship is found, which enables the identification of long distance transfer functions (where response measurements are too distant from the excitation location to achieve a sufficient signal to noise ratio), based on a series of shorter transfer FRF measurements.

It is noted that the round-trip formulation, alongside the proposed generalisation, do not require any additional assumptions over and above linearity and time-invariance [15]. Unlike alternative methods, the generalised round-trip applies to any complex built-up structure and, since no assumptions have been introduced, hypothetically reconstructs exact FRFs from in-situ experimental tests. In the search for an alternative approach, System Equivalent Model Mixing (SEMM) adopts the concept of frequency based sub-structuring to create a hybrid model for describing inaccessible and/or long distance transfer FRFs [16]. SEMM couples the dynamics of a measurement-based overlay model to the DoF-structure of an equivalent, yet not identical, parent model (e.g. full numerical models, analytical methods or detailed experimental DoF-models from a demonstrator study). Although SEMM can determine the structural dynamic properties at DoF other than the ones measured, the hybrid model requires some digital twin of the assembled structures while assuming shared boundary DoF between the models. While the aims of SEMM may be similar to those of the round-trip, they are fundamentally different concepts in that the former requires a model to reconstruct FRFs, whereas the latter achieves this solely from experimental data.

Given the above discussion, the remainder of this paper is structured as follows. Mathematical relations are presented in Section 2.1 to characterise transfer FRFs using an indirect 'round-trip journey'. Applications of this generalised theory for in-situ measurements of partially inaccessible transfer functions and noise reduction of long distance transfer paths are outlined in Sections 2.2 to 2.4, including concepts adopted from control theory to elaborate on practical considerations related to instrumentation. In Sections 3.1 and 3.2, both concepts are validated experimentally for multi-path, multi-DoF vibration problems.

2. Generalised round-trip identity for indirect FRF characterisation

This section presents a brief description of the coupled subsystems alongside the notation of the defined DoF followed by the derivation and practical implementations of the generalised round-trip identity, first, in Section 2.2 to indirect determination of transfer FRFs and secondly (Section 2.3) to 'long distance' FRFs.

The generalised round-trip concept is based on the source–receiver model shown in Fig. 1. In the assembly (C), an active subcomponent (A), containing some sort of internal source mechanism ($\boldsymbol{0}$) (e.g. electric motors, meshing gears, etc.), is connected to

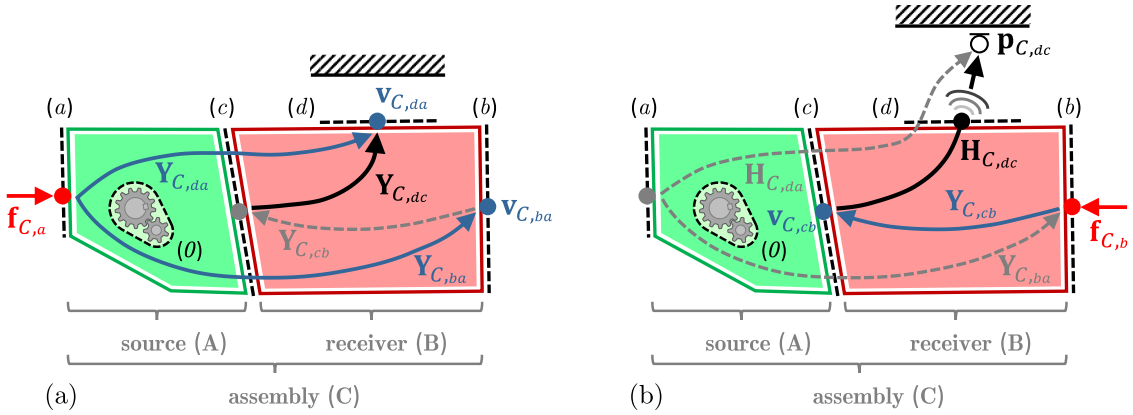

Fig. 1. Measurement steps to obtain the transfer path segments forming the generalised round-trip identity for the indirect characterisation of structural ($\mathbf{Y}_{C,dc}$) and vibro-acoustic ($\mathbf{H}_{C,dc}$) transfer functions. (a) - Step 1: Source-side excitation (a) to determine FRF terms to the receiver-side location (b) and the inaccessible target DoF (d). (b) - Step 2: Measurement of the receiver-side transfer function $\mathbf{Y}_{C,cb}$. For generality, the accelerometer at target (d) is replaced by a sound pressure probe.

the passive receiver (B) (e.g. mounting bracket, body panel, etc.). When operated, the source exerts dynamic forces and moments, through the coupling interface (c) (active–passive), onto the receiver; the latter simply propagates the induced vibration and/or radiates sound. Assembly (C) also contains remote locations on either side of the coupling interface, i.e. a set of accessible source-side DoF (a), accessible receiver-side DoF (b), and some target DoF (d) on the receiver. The target DoF (d) that may contain structural (see Fig. 1(a)) and/or sound pressure (see Fig. 1(b)) responses are considered encapsulated (illustrated by the hatched area), and are by definition inaccessible[1] for direct excitation. This source–receiver (active–passive) model, including a structure-borne source mechanism (0), is adopted from the TPA methodology, however, the round-trip concept applies equally to purely passive structures. The generalised round-trip formulation derived in the following section addresses the combined problem of providing an indirect relationship for structural $\mathbf{Y}_{C,dc}$ and vibro-acoustic $\mathbf{H}_{C,dc}$ transfer paths.

Note that the following discussion is based on the mobility concept, with the dependence on radian frequency ω omitted for clarity. It is stressed that any other FRF notation can be converted into mobility functions. For brevity, modifications to include vibro-acoustic FRFs are straightforward but not explicitly shown.

2.1. Generalisation of the round-trip relation

The following derivation is essentially the same as that in [15] but includes additional points remote from the interface at (d). First, consider the dynamic assembly (C) as illustrated in Fig. 1(a). For a harmonic input force applied to a single source-side DoF (a), the resultant velocities at the receiver locations (b) and the target DoF (d) are given by,

$$\mathbf{v}_{C,ba_i} = \mathbf{Y}_{C,ba}\,\mathbf{f}_{C,a_i} \tag{1}$$

$$\mathbf{v}_{C,da_i} = \mathbf{Y}_{C,da}\,\mathbf{f}_{C,a_i} \tag{2}$$

where $\mathbf{v}_{C,ba_i} = \left\{v_{C,b_1a_i},\, v_{C,b_2a_i},\, \ldots,\, v_{C,b_{n_b}a_i}\right\}^{\mathrm{T}}$ is the complex velocity response vector of the coupled assembly, denoted by the upper-case subscript 'C'. The lower-case subscripts 'a' and 'b' indicate the excitation and response DoF, respectively, including all n_b remote measurement positions (b) on the passive-side. A similar notation applies for the target response $\mathbf{v}_{C,da_i}$ at the remote locations (d). The external excitation f_{C,a_i} is arranged in the force vector $\mathbf{f}_{C,a_i} = \left\{0,\, \ldots,\, 0,\, f_{C,a_i},\, 0,\, \ldots,\, 0\right\}^{\mathrm{T}}$ and the subscript 'a_i' indicates the specific source-side excitation DoF.

Applying further excitations $(a_1, a_2, \ldots, a_{n_a})$ at other locations in (a) and arranging the columns into matrices yields the matrix equation,

$$\mathbf{V}_{C,ba} = \mathbf{Y}_{C,ba}\,\mathbf{F}_{C,a} \tag{3}$$

$$\mathbf{V}_{C,da} = \mathbf{Y}_{C,da}\,\mathbf{F}_{C,a}\,. \tag{4}$$

Here, the complex excitation matrix $\mathbf{F}_{C,a} = \left[\mathbf{f}_{C,a_1},\, \mathbf{f}_{C,a_2},\, \ldots,\, \mathbf{f}_{C,a_{n_a}}\right]$ contains the force vectors at each source DoF (a_i), resulting in the response matrices $\mathbf{V}_{C,ba} = \left[\mathbf{v}_{C,ba_1},\, \mathbf{v}_{C,ba_2},\, \ldots,\, \mathbf{v}_{C,ba_{n_a}}\right]$ and $\mathbf{V}_{C,da} = \left[\mathbf{v}_{C,da_1},\, \mathbf{v}_{C,da_2},\, \ldots,\, \mathbf{v}_{C,da_{n_a}}\right]$, respectively. Equating relations (3) and

[1] Reciprocal measurement of the vibro-acoustic counterpart requires excitation by a volume velocity source, which is also considered inaccessible.

(4), whilst eliminating $\mathbf{F}_{C,a}$, allows the following relation to be established,

$$\mathbf{V}_{C,da} = \underbrace{\mathbf{Y}_{C,da}\,\mathbf{Y}_{C,ba}^{-1}}_{\mathbf{T}_{C,db}^{(a)}}\,\mathbf{V}_{C,ba}\,. \tag{5}$$

Assuming the inverse to exist, which implies $n_a = n_b$, the product of the two mobility terms on the right-hand side of Eq. (5) formulates a generalised transmissibility term $\mathbf{T}_{C,db}^{(a)}$ [17]. In practice, additional excitation and/or response DoF may be included so as to over-determine the inverse problem, resulting in the inversion of a non-square matrix. In such a case, the Moore–Penrose pseudo inverse [18] is used to determine the least-squares solution, here the explicit notation '$^+$' is omitted for brevity.

The next stage in the derivation is to apply a force at the interface location (c), rather than at (a), so as to produce an identical response field in the receiver to that produced by $\mathbf{f}_{C,a_i}$. Although not intuitively obvious, it is now widely recognised [6,19] to the extent that it has been standardised in ISO 20270:2019 [7], that this force is none other than the blocked force of source substructure (A) when excited at (a). This force will be denoted $\overline{\mathbf{f}}_{A,c}$, the subscript 'A' denoting that it is a property of the source substructure alone and not influenced by the receiver substructure (B). The over-bar accent has been introduced to denote a blocked force, as opposed to a contact force. Full derivation is provided in [6] but a brief physical explanation is as follows: a force is applied at (a) producing a response field in the receiver; an additional force (a blocking force) is then applied at (c) so as to block the response at the interface and everywhere in the receiver; the force at (a) is then removed so that the original response field is reinstated in the receiver although reversed in sign. Because the receiver response is reduced to zero in the second step, the receiver dynamics have no influence and the blocking force is a property of the source alone.

In the context of structural responses, the equivalent blocked force excitation (compare Eqs. (1) and (2)) leads to,

$$\mathbf{v}_{C,ba} = -\mathbf{Y}_{C,bc}\,\overline{\mathbf{f}}_{A,c} \tag{6}$$

$$\mathbf{v}_{C,da} = -\mathbf{Y}_{C,dc}\,\overline{\mathbf{f}}_{A,c}\,. \tag{7}$$

Each applied force, denoted by the superscript '(a_i)', will result in a vector $\overline{\mathbf{f}}_{A,c}^{(a_i)} = \left\{\overline{f}_{A,c_1a_i}, \overline{f}_{A,c_2a_i}, \ldots, \overline{f}_{A,c_{n_c}a_i}\right\}^{\mathrm{T}}$ at interface (c); its rows correspond to specific coupling DoF $(c_1, c_2, \ldots, c_{n_c})$. Repeating the concept of Eqs. (3) and (4), multiple external excitations $(a_1, a_2, \ldots, a_{n_a})$ will result in sets of blocked force vectors, which may be arranged in columns of a blocked force matrix, $\overline{\mathbf{F}}_{A,c}$. The blocked force relation in Eqs. (6) and (7) can be extended by the matrix terms to,

$$\mathbf{V}_{C,ba} = -\mathbf{Y}_{C,bc}\,\overline{\mathbf{F}}_{A,c} \tag{8}$$

$$\mathbf{V}_{C,da} = -\mathbf{Y}_{C,dc}\,\overline{\mathbf{F}}_{A,c}\,. \tag{9}$$

The size of the complex blocked force matrix $\overline{\mathbf{F}}_{A,c} = \left[\overline{\mathbf{f}}_{A,c}^{(a_1)}, \overline{\mathbf{f}}_{A,c}^{(a_2)}, \ldots, \overline{\mathbf{f}}_{A,c}^{(a_{n_a})}\right]$ has become $n_c \times n_a$, including the full set of coupling DoF n_c and source excitations n_a. Substitution of Eqs. (8) and (9) into (5) yields the relation between the blocked force matrices,

$$\mathbf{Y}_{C,dc}\,\overline{\mathbf{F}}_{A,c} = \mathbf{Y}_{C,da}\,\mathbf{Y}_{C,ba}^{-1}\,\mathbf{Y}_{C,bc}\,\overline{\mathbf{F}}_{A,c}\,. \tag{10}$$

Provided that $\overline{\mathbf{F}}_{A,c}$ is full rank, both sides of Eq. (10) can be post-multiplied by its inverse yielding a generalised expression for the round-trip identity,

$$\mathbf{Y}_{C,dc} = \mathbf{Y}_{C,da}\,\mathbf{Y}_{C,ba}^{-1}\,\mathbf{Y}_{C,bc}\,. \tag{11}$$

The transfer function $\mathbf{Y}_{C,dc}$ is given by three alternative FRF matrices, none of which require direct excitation at the assumed inaccessible locations (c) or (d), respectively. Eq. (11) is the main result of this section. Following some simple rearrangements, the generalised round-trip identity features different applications as outlined in the next sections. Note that by moving points (d) to coincide with (c), i.e. identical DoF $(c) = (d)$, the standard form of the round-trip identity as given in [15] is obtained,

$$\mathbf{Y}_{C,cc} = \mathbf{Y}_{C,ca}\,\mathbf{Y}_{C,ba}^{-1}\,\mathbf{Y}_{C,cb}^{\mathrm{T}} \tag{12}$$

or by reciprocity,

$$\mathbf{Y}_{C,cc} = \mathbf{Y}_{C,cc}^{\mathrm{T}} = \mathbf{Y}_{C,cb}\,\mathbf{Y}_{C,ab}^{-1}\,\mathbf{Y}_{C,ca}^{\mathrm{T}} \tag{13}$$

limited to driving-point mobilities $\mathbf{Y}_{C,cc}$ at the coupling (active–passive) interface. In Fig. 2 the measurement procedure of the standard round-trip is schematised using a simplified source–receiver model omitting the separate set of remote target DoF (d).

2.2. Obtaining inaccessible transfer FRFs from indirect measurements

This section will focus on applying the generalised round-trip relation to enable indirect transfer function measurements of the assembly matrix, $\mathbf{Y}_{C,dc}$, between DoF at the source–receiver interface and any remote location downstream of it (i.e. on the receiver structure). To provide an entirely remote characterisation method for inaccessible transfer FRFs (the generalised round-trip is valid whether or not access is restricted), all excitations need to be relocated to accessible measurement positions. Here, 'inaccessible' refers to insufficient space to allow for an external excitation to be applied. It is assumed that the DoF (c) and (d) are still partly accessible for instrumentation (e.g. vibration sensors). In Eq. (11) the principle of reciprocity may be used to relocate the interface

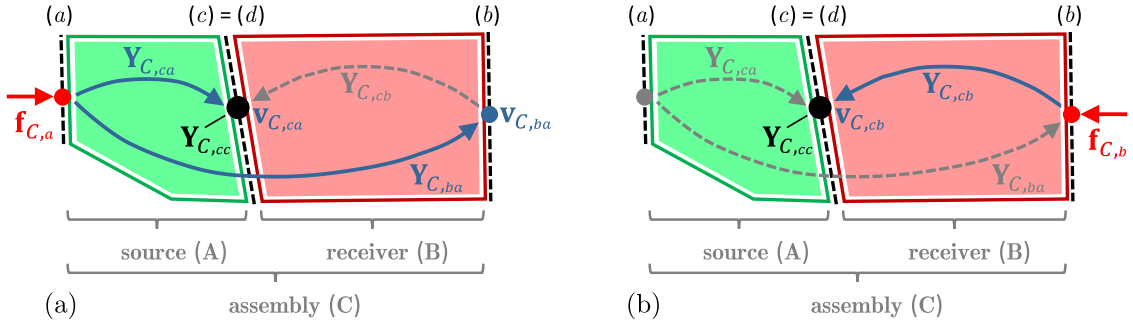

Fig. 2. Standard round-trip procedure with collocated DoF $(c) = (d)$, for indirect characterisation of inaccessible driving-point FRFs $\mathbf{Y}_{C,cc}$ at the coupling interface (c). External excitations are applied at source-side locations (a) and receiver-side remote points (b). (a) - Step 1: Source-side excitation (a) to determine the round-trip paths $\mathbf{Y}_{C,ca}$ and $\mathbf{Y}_{C,ba}$. (b) - Step 2: Receiver-side measurement of $\mathbf{Y}_{C,cb}$ from remote position (b).

excitations (c) to the accessible measurement positions at (b), $\mathbf{Y}_{C,bc} = \mathbf{Y}_{C,cb}^{\mathrm{T}}$ [10]. A practical formulation of the generalised round-trip is then given by,

$$\mathbf{Y}_{C,dc} = \mathbf{Y}_{C,da}\,\mathbf{Y}_{C,ba}^{-1}\,\mathbf{Y}_{C,cb}^{\mathrm{T}} \tag{14}$$

or by reciprocity,

$$\mathbf{Y}_{C,cd} = \mathbf{Y}_{C,dc}^{\mathrm{T}} = \mathbf{Y}_{C,cb}\,\mathbf{Y}_{C,ab}^{-1}\,\mathbf{Y}_{C,da}^{\mathrm{T}}\,. \tag{15}$$

Using the terminology of the 'round-trip journey' as introduced by Moorhouse [9], the mobility elements on the right-hand side of Eq. (14) frame $\mathbf{Y}_{C,dc}$ in a closed loop (see Fig. 1). This overview can be used as a practical guide to identify the two measurement steps required to obtain all three round-trip terms.

In the first step, the coupled structure is excited at the source-side DoF (a) while the receiver response is simultaneously measured at (b) and (d) to obtain $\mathbf{Y}_{C,ba}$ and $\mathbf{Y}_{C,da}$, respectively. The second step requires a force excitation on the passive side (b), while the resulting response is measured at the interface (c) to obtain the term $\mathbf{Y}_{C,cb}$. Note that the reciprocal relation in Eq. (15) reverses the path of $\mathbf{Y}_{C,ba}$, hence the measurements originate on the passive sub-structure (B). This converts the DoF at (b) to excitation-only points, whereas the positions at (a) are used for excitation and response measurement, alike. In practice, the target DoF (d) may function solely as response points (e.g. acceleration or sound pressure) without requiring any excitation. Even rotational DoF at either (c) or (d) may simply be included by specific sensor array setups at the interface and/or the target location. Along with the corresponding mathematical operation (e.g. finite difference approximation [20] or virtual point transformation [21]) translational responses from standard measurement accelerometers may be transformed to account for rotations in $\mathbf{Y}_{C,da}$ and/or $\mathbf{Y}_{C,cb}^{\mathrm{T}}$. As a result, this procedure enables the identification of structure-borne and/or vibro-acoustic transfer functions based on applied forces without special measurement equipment, such as moment exciters or volume velocity sources.

2.3. Improving long distance transfer FRFs by sectioned measurements

Instead of solely focusing on inaccessible driving-point and transfer FRFs the generalised round-trip concept may be applied to the identification of long distance transfer FRFs. In this section, the generalised round-trip relation is applied to establish a relation between the 'long' transfer term $\mathbf{Y}_{C,ba}$ measured across assembly (C) and shorter, yet equivalent, linking transfer FRFs.

For testing of civil, marine or other heavyweight structures, the excitation energy provided by a shaker or even a sledge impact hammer[2] might be insufficient to achieve an acceptable signal-to-noise ratio (SNR) on the response measurement. For such heavy and large structures, or other applications in which the response points are spaced too far apart from the non-collocated excitation, the round-trip journey in Eq. (11) can be re-arranged to combine shorter transfer functions to determine the long distance transfer path,

$$\mathbf{Y}_{C,ab} = \mathbf{Y}_{C,ba}^{\mathrm{T}} = \mathbf{Y}_{C,ad}\,\mathbf{Y}_{C,cd}^{-1}\,\mathbf{Y}_{C,cb}\,. \tag{16}$$

In this scenario, the targeted transfer function $\mathbf{Y}_{C,ab}$ shown in Fig. 3 spans across the entire assembly, whereas the indirect measurement is divided into three shorter path segments, each benefiting from an improved SNR on the individual response measurements. This reciprocal measurement technique requires response measurements at (a) and (c) while external force excitations are applied in two steps at (b) and (d), with (d) now being located at accessible measurement points. An effective way to improve the SNR of the long transfer function $\mathbf{Y}_{C,ab}$ is by defining additional receiver-side excitation locations (d) halfway along the targeted path, besides using high sensitivity measurement instrumentation.

[2] If sledgehammers or larger shakers are used to provide more energy, the risk to cause local deformation (i.e. non-LTI system) and/or the loss of spatial discretisation due to (enormous) hammer tips or larger shaker connectors can be avoided using the propose generalised round-trip approach.

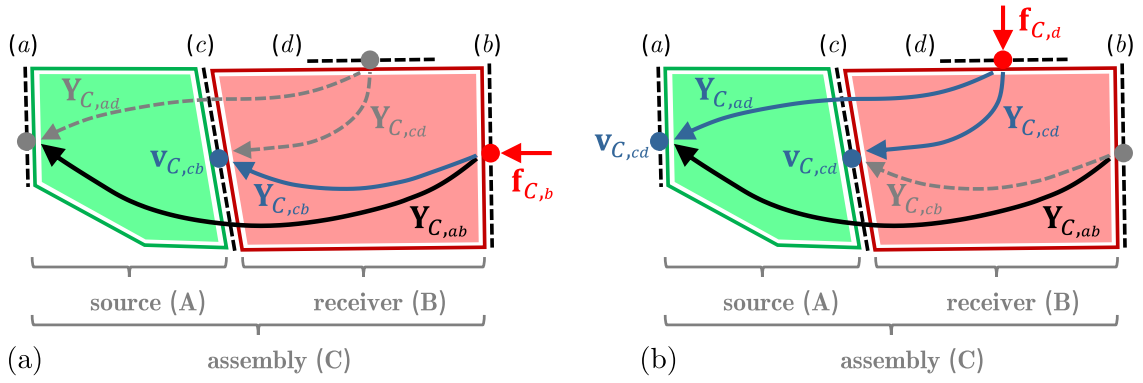

Fig. 3. Re-arranged transfer path segments of the generalised round-trip identity to improve measurement quality of long distance transfer functions $\mathbf{Y}_{C,ab}$ due to poor SNR or a high noise environment. (a) - Step 1: Receiver excitations at (b) to determine $\mathbf{Y}_{C,cb}$ (like actual reciprocal measurement of $\mathbf{Y}_{C,ab}$). (b) - Step 2: Excitation at arbitrary remote positions (d) to characterise $\mathbf{Y}_{C,ad}$ and $\mathbf{Y}_{C,cd}$.

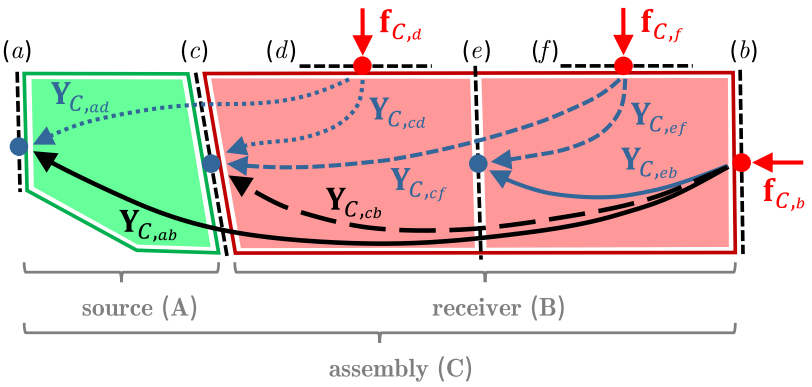

Fig. 4. Path segments of the long distance transfer FRF $\mathbf{Y}_{C,ab}$ using a nested generalised round-trip identity with 3 receiver-side excitation locations. The source–receiver model contains: target source DoF (a); coupling interface (c); virtual coupling interface (e); and remote DoF (d), (f), and (b) accessible for direct excitation.

In the case that access is available to the interface DoF (c), a similar long distance formulation can be obtained by collocating the DoF $(c) = (d)$,

$$\mathbf{Y}_{C,ab} = \mathbf{Y}_{C,ba}^{\mathrm{T}} = \mathbf{Y}_{C,ac}\,\mathbf{Y}_{C,cc}^{-1}\,\mathbf{Y}_{C,cb}\,. \tag{17}$$

To extend this concept, the round-trip equation can be applied recursively by nesting round-trip transfer FRFs within the identity in Eq. (16). Conceptually, the passive sub-component (B) of the source–receiver model may be sectioned by a virtual coupling interface (e). Introducing an additional set of accessible remote DoF (f) a recurring interface/remote DoF layout (i.e. $(c) - (d)$; $(e) - (f)$) is obtained, as depicted in Fig. 4.

Within the receiver sub-component (B), the separation of the coupling interface (c) and the remote DoF (b) by the virtual interface (e) bears a resemblance to the DoF configuration of the initial assembly (compare Fig. 3). Recalling the composed transfer FRF concept in Eq. (16), the receiver-side term $\mathbf{Y}_{C,cb}$ can be expressed by three shorter path segments,

$$\mathbf{Y}_{C,cb} = \mathbf{Y}_{C,cf}\,\mathbf{Y}_{C,ef}^{-1}\,\mathbf{Y}_{C,eb} \tag{18}$$

which requires direct force excitation at (f) and (b). The above relation may be nested, for instance, by substituting the receiver-side term $\mathbf{Y}_{C,cb}$ into the round-trip Eq. (16), thus including additional FRF terms in the long distance transfer function,

$$\mathbf{Y}_{C,ab} = \mathbf{Y}_{C,ba}^{\mathrm{T}} = \mathbf{Y}_{C,ad}\,\mathbf{Y}_{C,cd}^{-1}\,\mathbf{Y}_{C,cf}\,\mathbf{Y}_{C,ef}^{-1}\,\mathbf{Y}_{C,eb}\,. \tag{19}$$

The indirectly determined long distance transfer function $\mathbf{Y}_{C,ab}$ requires remote excitation at all 3 accessible DoF locations (d), (f), and (b).

In the case that the interface DoF (c) and (e) are accessible (compare Eq. (17)), the collocations $(c) = (d)$ and $(e) = (f)$ lead to the relation,

$$\mathbf{Y}_{C,ab} = \mathbf{Y}_{C,ba}^{\mathrm{T}} = \mathbf{Y}_{C,ac}\,\mathbf{Y}_{C,cc}^{-1}\,\mathbf{Y}_{C,ce}\,\mathbf{Y}_{C,ee}^{-1}\,\mathbf{Y}_{C,eb}\,. \tag{20}$$

Note that the collocated case requires the same instrumentation with accelerometers placed at (a), (c), and (e), like in the previous expression (see Eq. (19)), but now the external forces at (d) and (f) are relocated to the coupling interface (c) and the virtual interface (e), respectively.

This nested extension, implemented via virtual interfaces, is particularly beneficial for complex structures with long path segments, as shorter FRFs typically establish a strong phase relationship between the excitation measurement and the resulting response. This is partly due to a change in the nature of the wave propagation over long distances (e.g. standing wave to a travelling wave type), which causes the nested calculation to result in a long transfer function with a more reliable phase [22]. Positioned rather arbitrarily, multiple virtual interfaces may be considered to divide the receiver sub-component (B) in even smaller sections, thus improving the SNR and the phase relationship of the individual FRF measurements. However, the transfer segments are obtained from separate experiments, therefore, inconsistency encountered in the different experimental data may introduce errors in the predicted transfer FRFs [8].

2.4. Controllability and observability of the generalised round-trip relation

In practice, multi-contact assemblies often include translational and rotational coupling at interface (c). The question then arises as to how many remote DoF at (a), (b) and (d) are required to sufficiently perform the generalised round-trip identity for the multi-input multi-output (MIMO) case.

A requirement is defined by control theory [23], more specifically by the concepts of observability and controllability. Considering $\mathbf{Y}_{C,ba}$ of the inaccessible round-trip scenario (see Eq. (14)), the mutually independent force inputs at (a) are channelled through n_c DoF at interface (c) and transmitted to DoF (b) and (d) on the passive-side (see Fig. 5(a)). For $\mathbf{Y}_{C,ba}$ to be full rank and therefore invertible, the n_a source-side excitations $(a_1, a_2, \dots, a_{n_a})$ must each be applied in a different direction and position to ensure that all independent vibration modes at the interface (c) are excited. Controllability requires $n_a \geq n_c$ to obtain a sufficient contribution through all coupling DoF (n_c) from external excitations (n_a).

The notion of controllability can be understood by considering the contact forces present at interface (c) when excitations $\mathbf{F}_{C,a}$ are applied. Eq. (3) can be rewritten for the separated receiver sub-component (B) using the receiver mobility matrix $\mathbf{Y}_{B,bc}$ and the contact force matrix $\mathbf{F}_{B,c}$ applied at (c) [24],

$$\mathbf{V}_{C,ba} = \mathbf{Y}_{B,bc}\,\mathbf{F}_{B,c} \qquad \text{with} \qquad \mathbf{F}_{B,c} = (\mathbf{Y}_{A,cc} + \mathbf{Y}_{B,cc})^{-1}\,\mathbf{Y}_{A,ca}\,\mathbf{F}_{A,a}\,. \tag{21}$$

Note that the above subsystem expression considers excitations applied on the source sub-component, $\mathbf{F}_{A,a}$, hence the subscript of the excitation matrix $\mathbf{F}_{C,a}$ is replaced by 'A'. On the passive-side, the transmitted vibrations from independent external excitations (n_a in $\mathbf{F}_{C,a}$) are effectively limited by the number of interface/contact forces (n_c in $\mathbf{F}_{B,c}$). The interface reduces the independent response cases observed at (b) and, therefore, the effective rank of the mobility matrix $\mathbf{Y}_{C,ba}$ to a maximum of n_c. This constraint imposed by the coupling interface is regarded as a bottleneck effect [24]. The effect of the source excitation is observed on the receiving side by n_b remote DoF at (b). Whilst this may place further restrictions on the rank of $\mathbf{Y}_{C,ba}$, the observability condition requires $n_b \geq n_c$ to capture the entire set of interface dynamics of $\mathbf{F}_{B,c}$.

Assuming the external excitations at the source-side DoF (a) are mutually independent, it is best practice to define $n_a \geq n_b$. Theoretically, the rank n_r of the over-determined matrix $\mathbf{Y}_{C,ba}$ is limited by the number of linear independent responses n_b (rows of $\mathbf{Y}_{C,ba}$). Linear dependencies, resulting in a rank deficient matrix ($n_r < n_b$), indicate either that the assembly is identified to contain $n_c = n_r = \mathrm{rank}(\mathbf{Y}_{C,ba})$ DoF with the bottleneck effect actively restricting the number of independent excitations passing through the interface (c), or the inability of the source-side excitation n_a to excite all interface DoF n_c. To verify this, the effective rank can be analysed with a singular value decomposition (SVD). Additional source-side excitations, for instance using an instrumented hammer, may increase the number of significant singular values in $\mathbf{Y}_{C,ba}$, thus indicating insufficient controllability of the interface. Hence, additional excitations n_a (columns of $\mathbf{Y}_{C,ba}$) are required to improve the conditioning of $\mathbf{Y}_{C,ba}$ [24].

Consequently, full controllability and observability requires the round-trip identity in Eq. (14) to meet the condition $n_a \geq n_b \geq n_c$, whereas the reversed reciprocal relation in Eq. (15) must satisfy $n_b \geq n_a \geq n_c$. Both versions consider additional DoF at either (a) and/or (b), in other words, n_a may differ from n_b. For the non-square mobility matrix $\mathbf{Y}_{C,ba}$, the standard matrix inverse is then replaced by the Moore–Penrose pseudo inverse [18]. These conditions are independent of the number n_d of target DoF (d), which are defined as points requiring controlled interface dynamics $n_a \geq n_c$ (or by reciprocity: $n_b \geq n_c$) but are not essential for the observation of the interface dynamics. It is highlighted that despite the reference to and the restrictions by the number of coupling DoF (n_c), no explicit information is required about the interface DoF. The bottleneck constraint, imposed by the coupling condition, is independent of the sensor instrumentation at (c). Certain coupling DoF (e.g. rotational DoF) may be neglected completely in the accelerometer setup at (c) without changing the result of the predicted inaccessible transfer FRF [15].

Similar considerations of controllability and observability are adopted for the concept of long distance transfer FRF (see Eq. (16)), shown in Fig. 5(b). The external excitation (d) requires $n_d \geq n_c$ to fully control the interface dynamics, else $\mathbf{Y}_{C,cd}$ will be rank deficient and non-invertible. Limiting the number of independent vibration modes, the responses are observed at the interface itself, restricting the possibility to improve observability. At the same time, the instrumentation must include all coupling DoF through which physical coupling occurs, which may include in-plane and rotational DoF. For the collocated case (see Eq. (17)), the transfer FRF $\mathbf{Y}_{C,cd}$ reduces to a square symmetric matrix $\mathbf{Y}_{C,cc}$, thus requiring response and excitation measurements at all coupling DoF. For completeness, similar considerations apply to virtual interfaces of the nested extension, for instance $\mathbf{Y}_{C,ef}$ and $\mathbf{Y}_{C,ee}$ in Eqs. (19) and (20), respectively, as every interface may be associated with a virtual bottleneck effect. In contrast, the nature of external forces at (b) together with response measurement at (a) do not control or observe the interface dynamics and thus may be correctly placed at the targeted locations of the long distance transfer function.

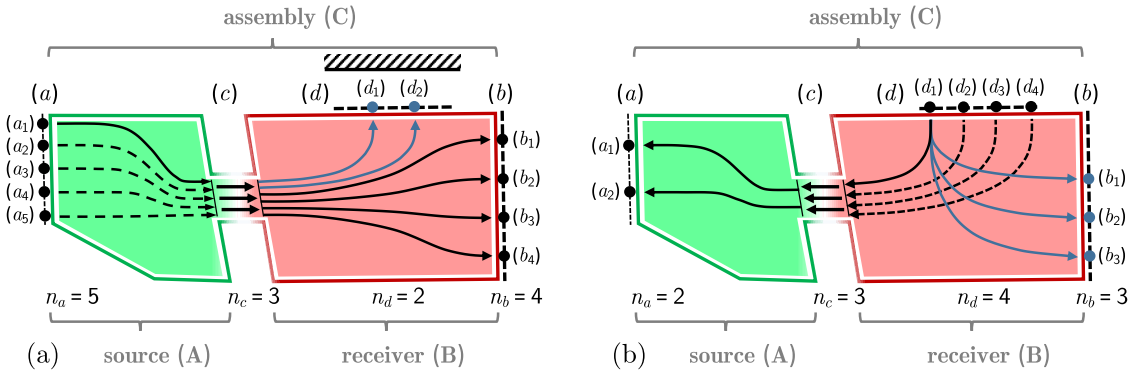

Fig. 5. Concept of controllability and observability effectively limiting the independent modes of vibration transmitted across the interface (bottleneck effect). (a) - Propagation model for inaccessible FRFs. (b) - Propagation model for long distance FRFs.

3. Experimental case studies

The previous sections introduced the generalised round-trip identity, whilst its implementation will vary depending on the context of the application. For the purpose of validation, the applications of the generalised round-trip identity will be demonstrated as part of two experimental multi-contact, multi-DoF examples. In the first example, the indirect approach outlined in Section 2.2 is adopted to characterise translational and rotational FRF terms inaccessible for direct force excitation. With previous works having focused on the theory and validation of the standard round-trip identity [11,25] (limited to driving-point FRFs), this Section will consider the generalised implementation for transfer functions with non-collocated excitation and response measurements. The second part considers long distance transfer FRFs of an automotive test bench setup, as proposed in Section 2.3, where additional force excitations at somewhat arbitrary receiver locations are applied to improve the measurement quality. In these experimental studies, a miniaturised shaker was used to apply broadband (white noise) force excitation for the FRF measurements. Alternatively, all FRFs may be obtained experimentally using impact excitations, however, the experimental uncertainty of roving hammer tests is highly subject to the skill of the experimentalist. In addition, the application of mini-shakers is preferred in this study since the force output can easily be controlled as required for the experiments described in Section 3.2.

3.1. Case study I: Beam-plate assembly - Multi-DoF characterisation of inaccessible transfer FRFs

This experimental section focuses on the ability of the round-trip concept to determine inaccessible transfer functions of a complex multi-DoF structure. A steel beam rigidly coupled to an aluminium plate (see Fig. 6(a)) was chosen so as to introduce sharp, minimally damped resonances, representative of what may be encountered in a worst-case practical scenario. The cross-like coupling elements (see Fig. 6(b)), denoted by (c_1) and (c_2), have been designed to facilitate characterisation of 6 DoF by using 2 bi-axial sensor pairs (separation distance $\triangle = 90$ mm). From the acceleration measurements, indicated by blue arrows, translational and angular responses are approximated in the central point of each cross using the finite difference approach [20].

The inaccessible transfer FRFs $\mathbf{Y}_{C,dc}$ are determined from all 12 DoF of the cross-like coupling elements (c_1) and (c_2) to the target tri-axial accelerometer (d) highlighted in yellow. Note that a wedge, as part of the receiver structure, rotates the direction of the target sensor to capture the structural response with a superposed contribution from all significant coupling DoF (c). Per definition, the sensor (d), located below the beam, and both coupling interfaces are inaccessible for direct force excitation prohibiting the direct measurement of the transfer functions.

The round-trip is calculated from 12 artificial source-side excitations (beam - (a)), depicted by red arrows, applied in different directions distributed over the entire beam to generate mutually independent excitations. The responses are observed downstream of the cross-like elements on the passive-side (plate - (b)) by 4 tri-axial accelerometers. Later, 12 additional excitations (a) and 3 remote response sensors (b), indicated in grey (see Fig. 6(a)), are used for an over-determination of the round-trip equation. The round-trip measurement procedure (**1**.-**3**.) including the validation process (*) may be outlined as follows:

1. The assembly matrices $\mathbf{Y}_{C,da} \in \mathbb{C}^{3\times12}$ and $\mathbf{Y}_{C,ba} \in \mathbb{C}^{12\times12}$ are measured simultaneously using a roving shaker approach (see Fig. 6(a)), with 12 excitations (red arrows) at different source-side locations (a) on the beam.
2. The matrix $\mathbf{Y}_{C,cb} \in \mathbb{C}^{12\times12}$ on the passive side is determined by direct force excitation on the accelerometers' faces at (b) and response measurements at the interface, indicated by blue arrows in Fig. 6(b).
3. Using the generalised round-trip formulation in Eq. (14), the inaccessible transfer FRFs $\mathbf{Y}_{C,dc} \in \mathbb{C}^{3\times12}$ are predicted from indirect measurements.

* To provide a validation method, reference FRFs are directly obtained from measurements of the cross-like elements. The tailored design allows force excitations for conventional FRF characterisation, depicted by red arrows in the inset of Fig. 6(a).

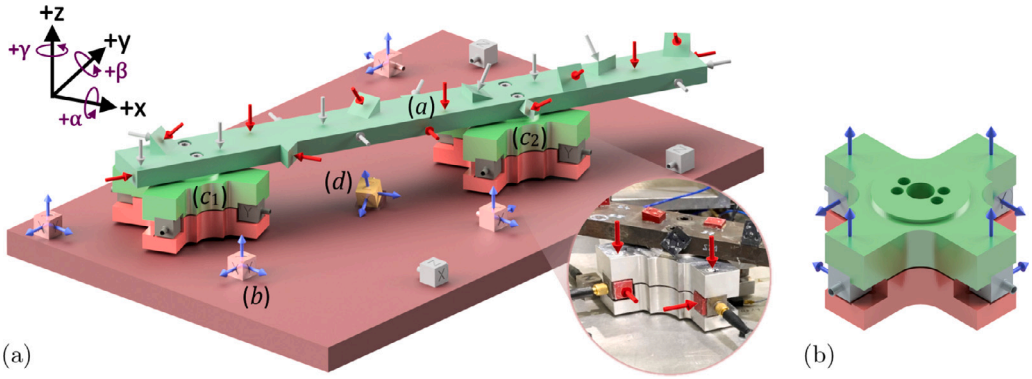

Fig. 6. Test structure for indirect determination of $\mathbf{Y}_{C,dc_1}$ and $\mathbf{Y}_{C,dc_2}$ between the cross-like coupling elements (c_1) and (c_2) and target positions (d) covered by the beam. Arrows indicate the excitation (red) and response (blue) measurements as utilised in the FRF reconstruction using the generalised round-trip concept, whilst excitations depicted in the close-up inset are required for the reference measurements. (a) - Multi-connection beam-plate assembly containing: beam — source (A); plate — receiver (B); cross-like elements with the coupling interfaces (c_1, c_2) being positioned exactly in its centre plane; inaccessible target responses (d). (b) - Cross-like interface, instrumented with 4 bi-axial accelerometers for finite difference approximation. (For interpretation of the references to colour in this figure legend, the reader is referred to the web version of this article.)

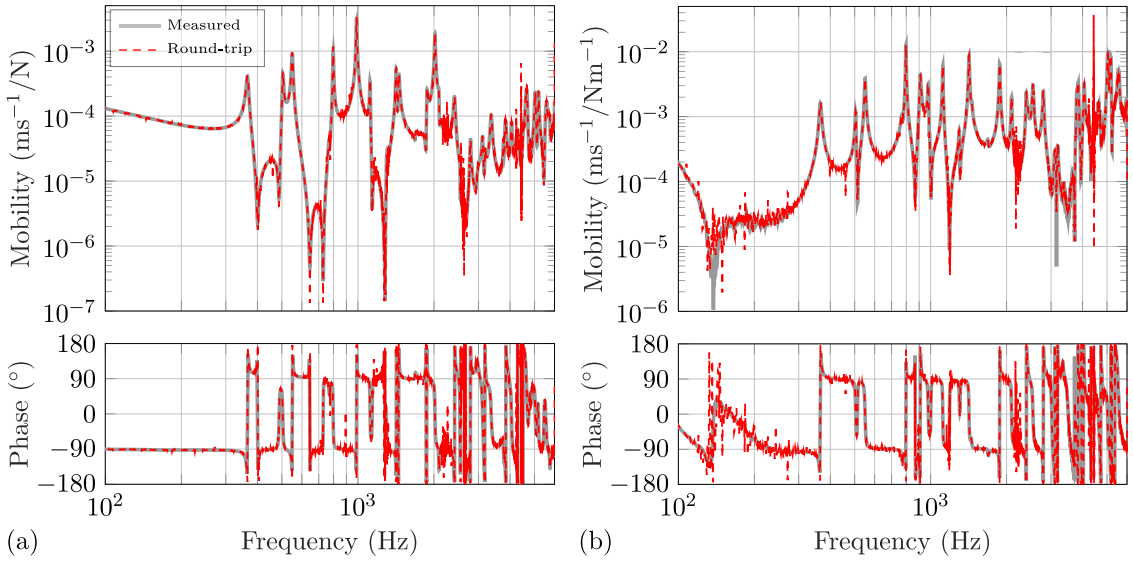

Fig. 7. Validation of inaccessible transfer functions using a determined system of equations ($n_a = n_b = n_c = 12$). Narrowband representation of the directly measured reference mobility (grey) compared to the indirect generalised round-trip identity (dashed red) for: (a) - Out-of-plane force excitation to target DoF, $Y_{C,dc}$ - $(d)/(c_{1z})$; (b) - In-plane moment excitation to target DoF, $Y_{C,dc}$ - $(d)/(c_{1\gamma})$.

Shown in Fig. 7 are the predicted transfer FRFs using the indirect generalised round-trip approach in Eq. (14) (dashed red), compared to the conventional validation measurement (grey). The selected transfer functions ($\mathbf{Y}_{C,dc} \in \mathbb{C}^{3\times12}$) displayed here describe the out-of-plane force (see Fig. 7(a)) and in-plane moment (see Fig. 7(b)) excitation at (c_1), whereas the target response is measured in the rotated out-of-plane direction (d). Over a multi-kHz range (100 Hz - 6 kHz) the reconstructed mobilities are in good agreement with the exact measurement, although influenced by undesired measurement noise of considerable magnitude in Fig. 7(b). This originates from the practical measurement setup, (see Fig. 6(a)): most excitations are pointing in the z-direction, which makes it difficult to excite the in-plane coupling DoF sufficiently and explains the higher deviations for the moment excitation.

With the highly resonant structure, which tends to cause poor conditioning, the encountered noise is the result of the determined assembly matrix $\mathbf{Y}_{C,ba}$ being ill-conditioned, and therefore severely affected by inversion errors. At lower frequencies the assembly's sensor array exhibits similar vibrations due to the long wavelength and thus results in some mutual dependence between columns of the corresponding FRF matrix. Inverse methods, such as the generalised round-trip approach considered in this work, are often susceptible to noise-induced errors and uncertainty arising from the experimental test procedure due to ill-conditioning. Although there exist numerical techniques to minimise this effect (e.g. regularisation), it is recommended that effort be spent acquiring reliable experimental data, as opposed to relying on such post-processing techniques. Nevertheless, even the most carefully executed

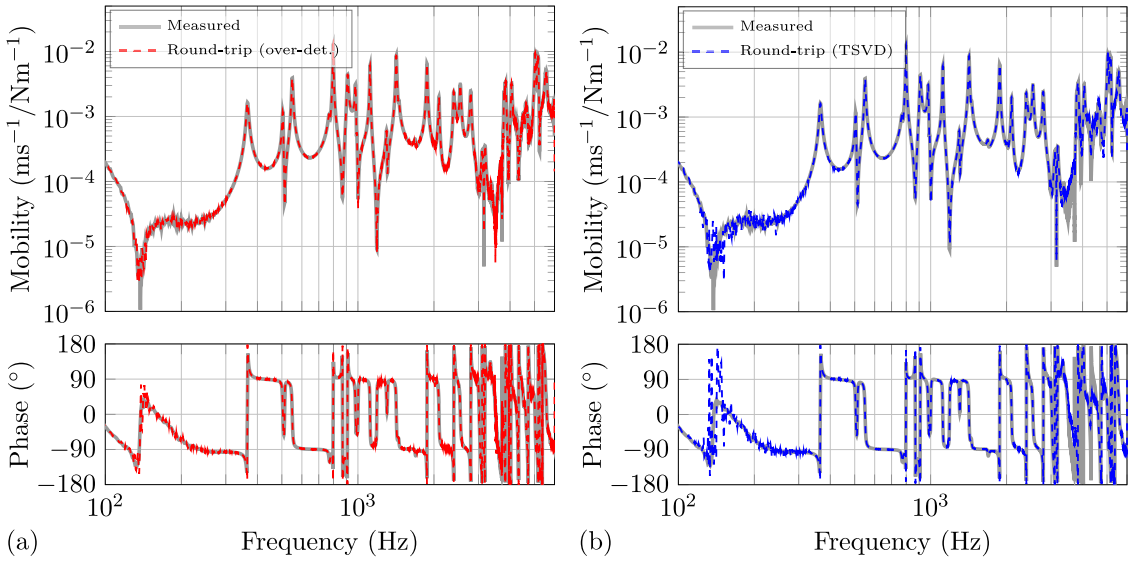

Fig. 8. Validation of the inaccessible transfer function using: (a) - Over-determined assembly matrix $\mathbf{Y}_{C,ba}$ with remote DoF ($n_a \geq n_b \geq n_c = 12$); (b) - Determined system matrix (see Fig. 7(b)) subject to singular value rejection. Narrowband representation for out-of-plane moment excitation at (c_1): directly measured reference (grey); over-determined generalised round-trip identity (dashed red); generalised round-trip identity using TSVD (dashed blue). (For interpretation of the references to colour in this figure legend, the reader is referred to the web version of this article.)

experiments will be subject to some degree of uncertainty. For a more detailed discussion, many works have focused on addressing this issue, particularly to reduce experimental uncertainty through methods such as over-determination or regularisation [26,27].

However, Eq. (14) does facilitate over-determination by including additional remote DoF at (a) and (b), respectively. As indicated in Fig. 6(a), 12 additional beam excitations and 3 tri-axial response sensors (depicted in grey) are considered in the amended mobility terms ($\mathbf{Y}_{C,da} \in \mathbb{C}^{3\times24}$; and $\mathbf{Y}_{C,cb} \in \mathbb{C}^{12\times21}$). This results in the inversion of a non-square, over-determined FRF matrix $\mathbf{Y}_{C,ba} \in \mathbb{C}^{21\times24}$. Hence, the standard matrix inverse is replaced by a Moore–Penrose pseudo inverse [18], leading to a least-squares solution of the problem likely to reduce inversion errors when implemented correctly. This over-determined mobility reconstruction is shown in Fig. 8(a) for the in-plane moment mobility. Over-determination of the inverse problem by a set of remote DoF ($n_a \geq n_b \geq n_c = 12$) provides a robust prediction by exceeding the minimum requirement for controllability and observability (see Section 2.4).

Alternatively, Fig. 8(b) shows the improvement of the moment mobility by a truncated singular value decomposition (TSVD) [28] of the initial determined system ($n_a = n_b = n_c = 12$). In this simple regularisation the two least significant singular values of $\mathbf{Y}^{-1}_{C,ba} \in \mathbb{C}^{12\times12}$ are rejected, since lower order singular values are likely composed of measurement error and noise. The truncated matrix inverse may be determined through the SVD factorisation of $\mathbf{Y}_{C,ba}$, given by,

$$\mathbf{Y}^{-1}_{C,ba} = \mathbf{V}\,(\mathbf{W}\boldsymbol{\Sigma})^{-1}\mathbf{U}^{\mathrm{T}} \qquad \text{with} \qquad \mathbf{W} = \left[\begin{array}{ccc|cc} 1 & 0 & 0 & 0 & 0 \\ 0 & \ddots & 0 & 0 & 0 \\ 0 & 0 & 1 & 0 & 0 \\ \hline 0 & 0 & 0 & 0 & 0 \\ 0 & 0 & 0 & 0 & 0 \end{array}\right] \in \mathbb{R}^{12\times12} \tag{22}$$

where the columns of $\mathbf{U}$ and $\mathbf{V}$ are the left and right singular vectors, respectively. The diagonal matrix $\boldsymbol{\Sigma} = \mathrm{diag}(\sigma_1, \sigma_2, \ldots, \sigma_{12})$ contains the singular values σ_i of $\mathbf{Y}_{C,ba}$ in descending order. The weighting matrix $\mathbf{W}$ effectively removes the two least contributing singular values (σ_{11} and σ_{12}) [26]. The truncated round-trip is obtained by substituting the regularised inverse formulation of Eq. (22) into Eq. (14). Therefore, without requiring additional instrumentation or experimental effort (compared to over-determination), the truncation significantly improves the result of the determined setup, although minor deviations occur between 3.3 kHz–5 kHz. This implies that the truncated singular values contain information about the structural dynamics, which are explicitly required to reconstruct the transfer mobility at high frequencies. Note that the results presented are, in a sense, based on a trivial rejection of 2 singular values, however, more sophisticated (also frequency dependent) approaches [29] may be adopted but are considered beyond the scope of this paper.

Considering the moment mobility in Fig. 8, both approaches significantly reduce noise to a level sufficient for most practical applications. The remaining noise between 100 Hz–300 Hz is likely caused by a finite difference error which may be resolved by a larger sensor spacing at the cross-like elements. The measured translational FRFs of the sensor pairs, which resolve the rotational DoF, are too similar[3] and thus the calculated difference of the spaced mobilities introduces noise [30]. This finite difference error,

[3] Especially at low frequencies, where the bending wavelength is very large compared to the accelerometer spacing, the measured mobilities at both sensor positions are, in fact, identical. Comparing such mobilities in the finite difference operation results in a noisy, unstable mobility approximation [30].

and perhaps the unreliability of measured mobilities at low frequencies, causes the actual reference measurement (grey) and the round-trip prediction (dashed red/blue) to contain similar errors.

For clarification, the accuracy of the indirect approach is independent of the number of computed transfer FRFs. With a particular interest in the translational terms of $\mathbf{Y}_{C,dc}$, incomplete interface instrumentation at (c_1) and (c_2) with single tri-axial accelerometers simplifies the experimental setup without impairing the accuracy of the result. As stressed in Section 2.4, the conditions of controllability and observability capture the system's dynamics, whereas $\mathbf{Y}_{C,cb}$ simply defines which transfer mobilities are computed depending on the sensor array (c) at the interface. However, the number of physical important coupling DoF at the rigid interface remains unchanged.

3.2. Case study II: Steering gear test setup - Characterisation of long distance transfer FRFs

This second study considers the application of the generalised round-trip identity to determine long distance transfer functions in multi-contact assemblies. The focus is on the measurement quality (i.e. SNR) rather than accessibility problems of certain DoF encountered by the experimentalist. The experimental setup, shown in Fig. 9, considers the long distance transfer functions between the motor mount of a Rack-and-pinion Electric Power Steering (REPS) system to the rigidly connected aluminium receiver plate (B). Cross-like elements (see Section 3.1) at each connection interface (c_1) and (c_2) are designed to fully determine 6 DoF coupling, including 3 translational and 3 rotational directions. The reciprocal measurement technique in Eq. (16) interchanges the excitation and response position of the non-collocated transfer function DoF, such that $\mathbf{Y}_{C,ab} = \mathbf{Y}^{\mathrm{T}}_{C,ba}$. Hence, the generalised round-trip measurements to identify the transfer properties between (a) and (b), including any validation FRF, originate from the passive-side with response measurement on the source-substructure (A).

To extend the distance between non-collocated DoF of the transfer FRFs, the remote force excitations (red arrows) at (b) are applied in the in-plane directions on a steel beam rigidly mounted to the receiver plate. On the source-side, the acceleration responses at (a) (blue arrows) are measured with 2 tri-axial accelerometers positioned at the motor mount. Unlike conventional transfer function measurements, where forces are applied one at a time to determine a single FRF, the generalised round-trip approach solves the MIMO system. However, implementation of the long distance approach in Eq. (16) requires additional instrumentation. The receiver-side is instrumented with 8 tri-axial accelerometers (d), (highlighted in yellow in Fig. 9) for remote response and excitation measurements. The duality of excitation and response at (d) requires easy access for roving hammer or shaker testing, which may be realised by practical sensor placement close to the structure's edges. FRF testing of this relatively large structure with stiff support stands in combination with a low in-plane dynamics of the plate-beam receiver requires considerable excitation energy to get an acceptable SNR on the response measurements. Hence, the remote DoF (d) are located in the vicinity of the support stands to define shorter path segments. As such, noise-sensitive measurements at (a), caused by the too distant force input at (b) and the high stiffness of the receiver sub-structure (B), can be avoided.

In this experimental study, all round-trip FRF elements are measured with a miniaturised shaker (see inset of Fig. 9) operated at about 30% of its maximum force output. The lowered shaker output is adjusted at the power amplifier stage to mimic an insufficient excitation scenario for the long transfer functions. However, operated at its full capacity, the 'high' excitation energy may be used to provide an appropriate reference measurement of $\mathbf{Y}_{C,ab}$. The generalised round-trip measurement procedure (**1**.-**3**.) at reduced shaker output, followed by the validation process (*) at full shaker output, may be outlined as follows:

1. The full distance FRFs $\mathbf{Y}_{C,ab} \in \mathbb{C}^{6\times 2}$ are measured at 'low' shaker output for a realistic representation of insufficient excitation. The applied force is adjusted to cause a poor SNR on the acceleration responses at (a), close the sensors' noise floor (Fig. 10(a)). Keeping the reduced amplifier settings unchanged, the matrix $\mathbf{Y}_{C,cb} \in \mathbb{C}^{12\times 2}$ is measured from shaker excitations on the accelerometer's faces at (b).
2. The assembly matrices $\mathbf{Y}_{C,ad} \in \mathbb{C}^{6\times 24}$ and $\mathbf{Y}_{C,cd} \in \mathbb{C}^{12\times 24}$ are determined simultaneously by roving shaker excitation, still at reduced energy output. The shaker forces are directly applied to the 24 (yellow) accelerometer surfaces at (d), depicted in the inset of Fig. 9.
3. The shorter transfer path segments are combined to determine the long distance transfer functions $\mathbf{Y}_{C,ab} \in \mathbb{C}^{6\times 2}$ using the generalised round-trip formulation in Eq. (16).

* The ideal full length reference FRFs are determined at maximum shaker output ('high power') by excitation on the remote sensor faces at (b), indicated by red arrows in Fig. 9.

Shown in Fig. 10(a) is the narrowband Fourier spectrum of the vibration response $\mathbf{v}_{C,ab}$ in the translational z-direction at the target motor mount (a) recorded during non-collocated shaker excitation at (b) under reduced power. By scaling the amplification factor of the shaker's force output, the attenuated vibration response (grey) falls near/below the sensitivity threshold (black) of the measurement equipment. The corresponding long distance transfer function $\mathbf{Y}_{C,ab}$ in Fig. 10(b) (grey) is, in fact, influenced by uncorrelated measurement noise at frequencies of poor SNR. Maintaining the 'low' shaker output, the compared result of the generalised round-trip procedure (dashed red) significantly improves the FRF quality. Reconstructed from shorter path segments, anti-resonances are more prominent in the reconstructed FRF, aside from noise being attenuated, as depicted in the inset from 1.1 kHz–1.4 kHz.

The actual experimental validation of the above generalised round-trip procedure (dashed red) is provided in Fig. 11(a) through a comparison of the long distance FRF with a direct reference measurement at 'high' shaker output (black). The round-trip method provides a convincing agreement, however, some measurement noise still remains especially at low frequencies between 170 Hz–370 Hz, highlighted in the inset. The artificially lowered shaker output for the round-trip measurement campaign fails to determine

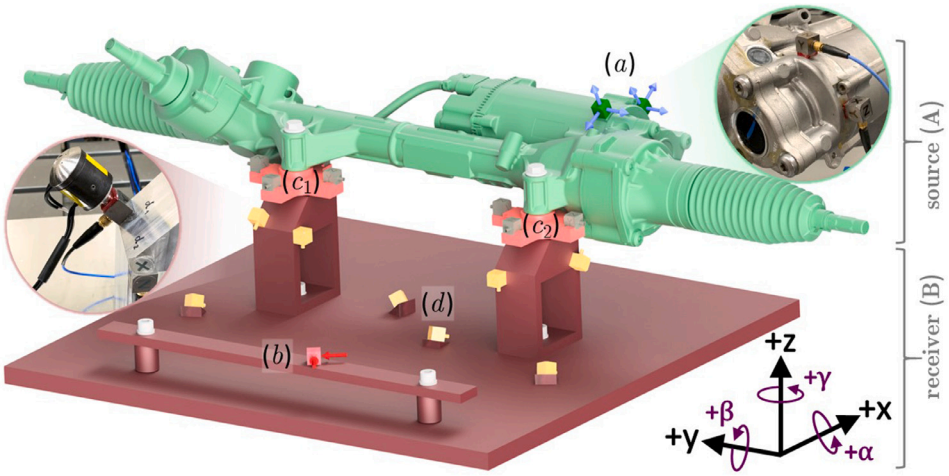

Fig. 9. Test structure forming a long distance transfer function $\mathbf{Y}_{C,ab}$ from the remote position (b) on the beam to the motor mount (a). Arrows indicate the excitation (red) and response (blue) measurements of the conventional transfer function characterisation, whilst the shaker excitation at (d), depicted in the close-up inset, is part of the generalised round-trip identity. The source–receiver setup contains: REPS — source (A); plate-beam assembly — receiver (B); cross-like elements — coupling interfaces (c_1, c_2); remote locations (d) accessible for direct excitation. (For interpretation of the references to colour in this figure legend, the reader is referred to the web version of this article.)

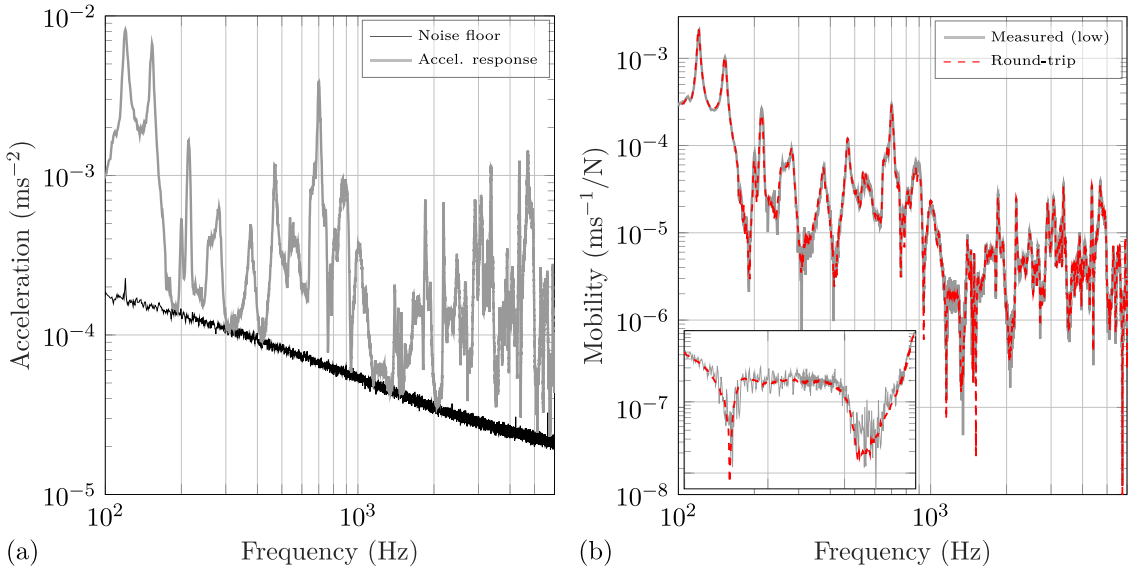

Fig. 10. Insufficient SNR from low level shaker excitation at the receiver-side (b). Narrowband representation: (a) - Acceleration response (grey) at the motor mount (a) close to the sensor's noise floor (black). (b) - Directly measured long distance transfer function $\mathbf{Y}_{C,ba}$ considerably contaminated by noise resulting from the 'low/insufficient' shaker excitation (grey) and improvement by the generalised round-trip (dashed red) concept. (Inset covers frequency range from 1.1–1.4 kHz).

all mobility elements with a sufficient SNR completely free from measurement noise. A relocation of the remote positions (d) or, alternatively, a virtual interface (see Fig. 4) may be introduced and used in conjunction with the nested round-trip formulation in Eq. (19) to improve measurement quality at anti-resonances.

The result of a more simplistic instrumentation setup with fewer accelerometers and less measurement effort is shown in Fig. 11(b). The dynamics at the coupling interface, for instance, are characterised by 3 translational DoF each ($n_c = 6$), which theoretically reduces the finite difference sensor array to a simple tri-axial accelerometer mounted to each foot (c_1 and c_2). Clearly, the reduced interface description benefits the receiver-side instrumentation at (d), with 12 excitations on 4 sensors providing a 2 fold over-determination of $\mathbf{Y}_{C,cd} \in \mathbb{C}^{6\times12}$. The considerably reduced experimental effort comes at the disadvantage of inaccuracies in the frequency range between 170 Hz–370 Hz (see inset of Fig. 11(b)) worsening at higher frequencies. The incomplete representation of the coupling interface dynamics is limited to translational DoF only, while rotational coupling in the transmissibility term $\mathbf{T}^{(c)}_{C,bd} = \mathbf{Y}^{-1}_{C,cd}\,\mathbf{Y}_{C,cb}$ is mathematically omitted. Although the mobility term $\mathbf{Y}_{C,ad}$ (see Eq. (16)) implicitly includes the complete

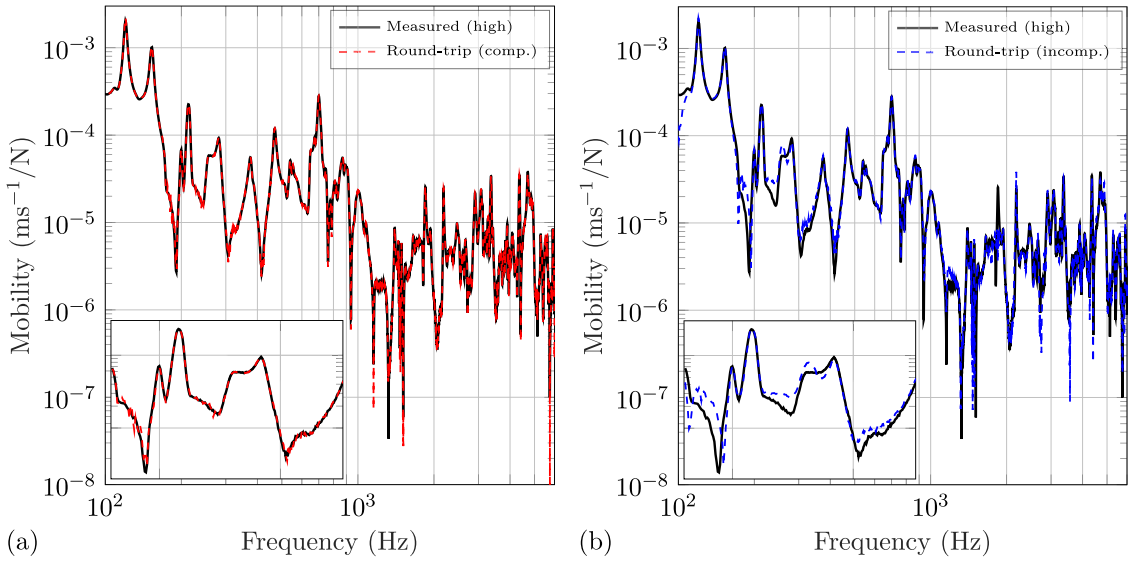

Fig. 11. Validation of the long distance transfer function based on: (a) - Complete description of the coupling interface (c) (see Fig. 10(b)) including rotational and translational coupling DoF ($n_c = 12$; finite-difference approximation); (b) - Translational coupling only ($n_c = 6$; e.g. tri-axial sensor). Narrowband representation of $Y_{C,ba}$: directly measured reference at 'high' shaker output (black); generalised round-trip identity with fully described interface (dashed red); generalised round-trip identity using an incomplete interface characterisation (dashed blue). (Inset covers frequency range from 170–370 Hz). (For interpretation of the references to colour in this figure legend, the reader is referred to the web version of this article.)

set of DoF through which physical coupling occurs, rotational transfer paths are not included in the propagating transmissibility term.

Note that care should be taken when certain DoF are neglected in the system description. Although the simplification in Fig. 11(b) yields a rather accurate result, other structures may be more dependent on rotational coupling causing major deviations. However, the structure's sensitivity to an incomplete interface description can be assessed with the coherence-style Interface Completeness Criterion (ICC) [2,8].

4. Conclusions

This paper has been concerned with the indirect characterisation of structural and/or vibro-acoustic frequency response functions. Applications include the identification of FRFs whose excitation and response positions are inaccessible for direct measurement, and to improve the measurement quality of long distance transfer functions. A generalised round-trip relation has been presented, where assembly FRFs are expressed by three alternative FRF terms, altogether forming a closed 'round-trip journey'.

As an entirely remote identification method, the generalised round-trip identity may be used to determine inaccessible transfer functions of an assembly, whereby all inaccessible excitations are relocated to accessible remote locations. In practice, simple response measurements at both non-collocated positions of the transfer functions have been used for the indirect characterisation, while spaced accelerometer pairs facilitate finite difference approximation to consider rotational coupling at the interface. Over a multi-kHz frequency range, the generalised round-trip approach, when implemented correctly, offers more flexibility for practical system characterisation when conducted in-situ. The advantage of a complete FRF characterisation, including all DoF (e.g. in-plane, rotational), comes at little costs in terms of additional experimental effort and instrumentation. Thus, direct impact measurements of poorly accessible locations, prone to insufficient coherence, may be avoided. Integrated as part of a TPA procedure, these transfer FRFs may be used to propagate a blocked force source output to facilitate: rank ordering of source contributions, sound and vibration prediction in physical structures (in-situ TPA), or in virtual environments (component-based TPA/VAP).

By rearrangement of the generalised round-trip identity, a relation for long distance transfer functions has been identified. Based on shorter path segments the round-trip reconstruction has been found to improve measurement quality in scenarios where conventional FRF testing provides insufficient SNR. The reconstruction from sectioned FRF terms enables a second external excitation halfway along the transfer path to amplify the structural response. Depending on the arbitrary yet accessible second excitation position on the receiver-side, the shorter transfer function segments may benefit from a higher SNR, a stronger phase relation, and a better coherence. Once instrumented, this MIMO technique enables characterisation of non-collocated FRFs between distant input/output pairs, for instance, resiliently mounted source components that cause the vibration response of the conventional FRF measurement to fall below the sensitivity threshold of the available measurement equipment.

Practical instrumentation guidelines have been provided based on control theory for MIMO systems and notions of controllability and observability for transmitted vibrations restricted by the interface's bottleneck effect (active–passive). It is important to reiterate that the generalised round-trip requires an FRF matrix inversion, which has been addressed on a theoretical and experimental basis.

For collocated locations of (c) and (d), such that $(c) = (d)$, the proposed round-trip formulates a driving-point matrix relation, which is in exact agreement with the standard round-trip identity [11]. The target DoF (d) may also be interpreted as a second, virtual interface, hence the proposed 'generalised expression' combines both special cases of the standard and dual interface round-trip scenario [13] and, furthermore, allows for a determination of passive properties for the complete assembly downstream the source.

CRediT authorship contribution statement

K. Wienen: Conceptualization, Methodology, Validation, Investigation, Writing - original draft, Writing - review & editing. **M. Sturm:** Writing - review & editing, Supervision, Resources. **A.T. Moorhouse:** Writing - review & editing, Supervision, Project administration. **J.W.R. Meggitt:** Writing - review & editing, Supervision.

Declaration of competing interest

The authors declare that they have no known competing financial interests or personal relationships that could have appeared to influence the work reported in this paper.

References

[1] A.S. Elliott, A.T. Moorhouse, T. Huntley, S. Tate, In-situ source path contribution analysis of structure borne road noise, J. Sound Vib. 332 (24) (2013) 6276–6295, http://dx.doi.org/10.1016/j.jsv.2013.05.031.
[2] K. Wienen, M. Sturm, A.T. Moorhouse, J.W.R. Meggitt, Robust NVH engineering using experimental methods - Source characterization techniques for component transfer path analysis and virtual acoustic prototyping, in: SAE Technical Papers, Grand Rapids, USA, 2019. http://dx.doi.org/10.4271/2019-01-1542.
[3] M. Sturm, T.H. Alber, A.T. Moorhouse, D. Zabel, Z. Wang, The in-situ blocked force method for characterization of complex automotive structure-borne sound sources and its use for virtual acoustic prototyping, in: Proceedings of the International Conference on Noise and Vibration Engineering - ISMA, Leuven, Belgium, 2016.
[4] D. de Klerk, D.J. Rixen, S.N. Voormeeren, General framework for dynamic substructuring: history, review and classification of techniques, AIAA J. 46 (5) (2008) 1169–1181, http://dx.doi.org/10.2514/1.33274.
[5] J.W.R. Meggitt, A.T. Moorhouse, K. Wienen, M. Sturm, A framework for the propagation of uncertainty in transfer path analysis, J. Sound Vib. 483 (2020) 115425, http://dx.doi.org/10.1016/j.jsv.2020.115425.
[6] A.T. Moorhouse, A.S. Elliott, T.A. Evans, In situ measurement of the blocked force of structure-borne sound sources, J. Sound Vib. 325 (4–5) (2009) 679–685, http://dx.doi.org/10.1016/j.jsv.2009.04.035.
[7] International Organization for Standardization, ISO 20270:2019 Acoustics - Characterization of sources of structure-borne sound and vibration - Indirect measurement of blocked forces, 2019.
[8] J.W.R. Meggitt, A.T. Moorhouse, On the completeness of interface descriptions and the consistency of blocked forces obtained in situ, Mech. Syst. Signal Process. 145 (2020) 106850, http://dx.doi.org/10.1016/j.ymssp.2020.106850.
[9] A.T. Moorhouse, A.S. Elliott, Indirect measurement of frequency response functions applied to the problem of substructure coupling, in: Proceedings of Noise and Vibration: Emerging Methods - NOVEM, Sorrento, Italy, 2012.
[10] F.J. Fahy, Some applications of the reciprocity principle in experimental vibroacoustics, Acoust. Phys. 49 (2) (2003) 217–229, http://dx.doi.org/10.1134/1.1560385.
[11] A.T. Moorhouse, T.A. Evans, A.S. Elliott, Some relationships for coupled structures and their application to measurement of structural dynamic properties in situ, Mech. Syst. Signal Process. 25 (5) (2011) 1574–1584, http://dx.doi.org/10.1016/j.ymssp.2010.12.016.
[12] A.P. Urgueira, R.A. Almeida, N.M. Maia, On the use of the transmissibility concept for the evaluation of frequency response functions, Mech. Syst. Signal Process. 25 (3) (2011) 940–951, http://dx.doi.org/10.1016/j.ymssp.2010.07.015.
[13] J.W.R. Meggitt, A.S. Elliott, A.T. Moorhouse, H.K. Lai, In situ determination of dynamic stiffness for resilient elements, Proc. Inst. Mech. Eng. C 230 (6) (2016) 986–993, http://dx.doi.org/10.1177/0954406215618986.
[14] J.W.R. Meggitt, A.T. Moorhouse, In-situ sub-structure decoupling of resiliently coupled assemblies, Mech. Syst. Signal Process. 117 (2019) 723–737, http://dx.doi.org/10.1016/j.ymssp.2018.07.045.
[15] A.T. Moorhouse, A.S. Elliott, The "round trip" theory for reconstruction of green's functions at passive locations, J. Acoust. Soc. Am. 134 (5) (2013) 3605–3612, http://dx.doi.org/10.1121/1.4821210.
[16] S.W. Klaassen, M.V. van der Seijs, D. de Klerk, System equivalent model mixing, Mech. Syst. Signal Process. 105 (2018) 90–112, http://dx.doi.org/10.1016/j.ymssp.2017.12.003.
[17] A.M.R. Ribeiro, J.M.M. Silva, N.M.M. Maia, On the generalisation of the transmissibility concept, Mech. Syst. Signal Process. 14 (1) (2000) 29–35, http://dx.doi.org/10.1006/mssp.1999.1268.
[18] R. Penrose, J.A. Todd, A generalized inverse for matrices, Math. Proc. Camb. Phil. Soc. 51 (3) (1955) 406–413, http://dx.doi.org/10.1017/S0305004100030401.
[19] M.V. van der Seijs, D. de Klerk, D.J. Rixen, General framework for transfer path analysis: History, theory and classification of techniques, Mech. Syst. Signal Process. 68–69 (2016) 217–244, http://dx.doi.org/10.1016/j.ymssp.2015.08.004.
[20] A.S. Elliott, A.T. Moorhouse, G. Pavić, Moment excitation and the measurement of moment mobilities, J. Sound Vib. 331 (11) (2012) 2499–2519, http://dx.doi.org/10.1016/j.jsv.2012.01.022.
[21] M.V. van der Seijs, D. van den Bosch, D.J. Rixen, D. de Klerk, An improved methodology for the virtual point transformation of measured frequency response functions in dynamic substructuring, in: Proceedings of the 4th ECCOMAS Thematic Conference on Computational Methods in Structural Dynamics and Earthquake Engineering, Kos Island, Greece, 2014. http://dx.doi.org/10.7712/120113.4816.C1539.
[22] J.W.R. Meggitt, On In-Situ Methodologies for the Characterisation and Simulation of Vibro-Acoustic Assemblies (Ph.D. thesis), University of Salford, UK, 2017.
[23] A. Preumont, in: J.R. Barber, A. Klarbring, G.M.L. Gladwell (Eds.), Vibration Control of Active Structures, fourth ed., Springer International Publishing, Cham, 2018, http://dx.doi.org/10.1007/978-3-319-72296-2.
[24] M.V. van der Seijs, Experimental Dynamic Substructuring Analysis and Design Strategies for Vehicle Development (Ph.D. thesis), Delft University of Technology, Netherlands, 2016.

[25] C. Höller, B.M. Gibbs, Indirect determination of the mobility of structure-borne sound sources, J. Sound Vib. 344 (2015) 38–58, http://dx.doi.org/10.1016/j.jsv.2015.01.011.
[26] A. Thite, D. Thompson, The quantification of structure-borne transmission paths by inverse methods. Part 1: Improved singular value rejection methods, J. Sound Vib. 264 (2003) 411–431, http://dx.doi.org/10.1016/S0022-460X(02)01202-6.
[27] A. Thite, D. Thompson, The quantification of structure-borne transmission paths by inverse methods. Part 2: Use of regularization techniques, J. Sound Vib. 264 (2003) 433–451, http://dx.doi.org/10.1016/S0022-460X(02)01203-8.
[28] A.T. Moorhouse, Compensation for discarded singular values in vibro-acoustic inverse methods, J. Sound Vib. 267 (2) (2003) 245–252, http://dx.doi.org/10.1016/S0022-460X(02)01432-3.
[29] H.W. Engl, M. Hanke, A. Neubauer, Regularization of Inverse Problems, first ed., Kluwer Academic Publishers, Dordrecht, 2000.
[30] A.S. Elliott, G. Pavić, A.T. Moorhouse, Measurement of force and moment mobilities using a finite difference technique, in: Proceedings of EURONOISE, Paris, France, 2008. http://dx.doi.org/10.1121/1.2933757.